

The Curious Magnetic Properties of Orbital Chern Insulators

Jihang Zhu,¹ Jung-Jung Su,² and A.H. MacDonald¹

¹Department of Physics, University of Texas at Austin, Austin TX 78712

²Department of Electrophysics, National Chiao Tung University, Hsinchu 300, Taiwan

Chern insulator ferromagnets are characterized by a quantized anomalous Hall effect, and have so far been identified experimentally in magnetically-doped topological insulator (MTI) thin films and in bilayer graphene moiré superlattices. We classify Chern insulator ferromagnets as either spin or orbital, depending on whether the orbital magnetization results from spontaneous spin-polarization combined with spin-orbit interactions, as in the MTI case, or directly from spontaneous orbital currents, as in the moiré superlattice case. We argue that in a given magnetic state, characterized for example by the sign of the anomalous Hall effect, the magnetization of an orbital Chern insulator will often have opposite signs for weak n and weak p electrostatic or chemical doping. This property enables pure electrical switching of a magnetic state in the presence of a fixed magnetic field.

Introduction—A ferromagnet may be defined as an equilibrium state of matter in which time-reversal (TR) symmetry is broken without lowering translational symmetries. Ferromagnets generically have both non-zero spin magnetization and non-zero orbital magnetization. In almost all ferromagnets, the microscopic mechanism responsible for order is spontaneous spin-alignment driven by exchange interactions, which breaks spin-rotational invariance and leads to a non-zero spatially averaged spin moment density. Spin-orbit interactions then play a weak role by inducing a small parasitic contribution to magnetization from orbital currents and a related non-zero (anomalous) Hall conductivity.

This Letter is motivated by recent experiments[1–4] that have established the quantized anomalous Hall effect (QAHE) in two quite different classes of two-dimensional ferromagnets. The QAHE signals[5, 6] the formation of a ferromagnetic state, often referred to as a Chern insulator, with occupied quasi-particle bands whose topological Chern numbers[7] summed to a non-zero value. We find that when ferromagnetism results from spontaneous orbital moments (not spin moments), as in the QAHE states recently discovered[2–4] in magic angle twisted bilayer graphene (MATBG), the magnetizations of weakly n -doped and weakly p -doped insulators can differ in sign in the same magnetic state, characterized for example by a given sign of the anomalous Hall conductivity. This property could enable magnetic state reversal in the presence of a magnetic field to be achieved purely electrically.

The mechanism that allows the magnetizations of weakly n -doped and weakly p -doped Chern insulators to differ drastically is closely related to the quantum Hall effect itself. Because of the presence of protected edge states, the orbital magnetization M of a Chern insulator changes[8] with chemical potential μ even when μ is inside the bulk energy gap:

$$\frac{dM}{d\mu} = \frac{1}{c} \frac{dI}{d\mu} = \frac{Ce}{2\pi\hbar c}, \quad (1)$$

where C , the Chern index sum, is an integer equal to the Hall conductance in e^2/h units. Eq. (1) emphasizes that the quantized Hall conductance can be understood[8] in terms of chiral edge states that are occupied to different chemical potentials along different portions of the sample boundary. It follows from Eq. (1) that the bulk magnetization jumps

by $\Delta M = CeE_{\text{gap}}/2\pi\hbar c$ when the chemical potential jumps across the gap of a Chern insulator. Note that the jump in the magnetization depends only on the value of the energy gap and on fundamental constants. We show below that in orbital Chern insulator ferromagnets this jump can be sufficient to change the sign of magnetization simply by changing the sign of doping.

Spin Chern Insulators—In magnetically doped topological insulator thin films, TR symmetry is broken by introducing local moments that order ferromagnetically. Spin-orbit coupling then leads to an anomalous Hall effect that is quantized, and to orbital ferromagnetism. To compare the orbital magnetization jump with the magnitude of the spin magnetization, we express it in units of Bohr magnetons ($\mu_B = e\hbar/2mc$) per surface unit cell:

$$\frac{\Delta M}{\mu_B/A_{\text{uc}}} = \frac{CmA_{\text{uc}}E_{\text{gap}}}{\pi\hbar^2} \quad (2)$$

where A_{uc} is the area of the surface unit cell. In magnetically doped topological insulators, spin magnetization in Bohr magnetons per surface unit cell is typically ~ 1 , because the fraction of sites with magnetic atoms is ~ 0.1 and the number of magnetically doped layers is ~ 10 . Note that the spin magnetization does not depend on the position of the chemical potential within the gap. We see from Eq. (2) that the jump in the orbital magnetization across the gap is small by comparison with the spin magnetization since the surface state energy gap E_{gap} , although not known accurately, is certainly small compared to the \hbar^2/mA_{uc} , which depends only on fundamental constants and the surface unit cell area and has a typical value in the 1 – 10 eV range. For magnetically doped topological insulators, and other spin Chern insulators, the unusual jump in the magnetization across the insulator's gap is small in a relative sense and unlikely to have a qualitative influence on magnetic properties.

Orbital Chern Insulators—The Hall conductivity of a Chern insulator ferromagnet is quantized when the chemical potential lies in the gap or when carriers introduced by chemical or electrostatic doping are localized. It is convenient to use the sign of the Hall conductivity to distinguish a magnetic state from its TR counterpart. We will refer to the state with positive quantized Hall conductivity Ce^2/h as the + state and to the

state with negative quantized Hall conductivity $-Ce^2/h$ as the $-$ state. Although their variations with chemical potential are very distinct, as we emphasize below, both the Hall conductivity $\sigma_H^\pm(\mu)$ and orbital magnetization $M^\pm(\mu)$ are orbital fingerprints of broken TR and at any doping level have opposite signs in TR partner states: $M^-(\mu) = -M^+(\mu)$, $\sigma_H^-(\mu) = -\sigma_H^+(\mu)$.

The TR symmetry breaking mechanism active in the orbital Chern insulators recently discovered in MATBG devices is almost certainly condensation in momentum space, a concept discussed some time ago by Heisenberg and London[9] and recently proposed[10] as a possible symmetry breaking mechanism in metallic gated bilayer graphene. Momentum space condensation is driven by the property that interaction energies in systems with long-range Coulomb interactions can be lowered by occupying states that are more compactly distributed in momentum space than the occupied states of non-interacting bands. Just as exchange interactions in itinerant electron systems occur only between like spins, exchange interactions between states with nearby momenta are stronger than those between states far apart in momentum space. In materials, like graphene, with low energy states located near two widely separated valley centers, momentum space condensation translates to spontaneous valley population polarization. When combined with the intrinsically topological character[11–13] of the valley-projected bands in these materials, valley polarization yields an AHE that is quantized in insulating states. The recently discovered graphene multilayer QAHE states[2–4] provide, as far as we are aware, the only demonstrated example of this mechanism at work. In order to estimate the orbital magnetization of these states we apply the convenient envelope function description[14] in which the moiré superlattices is described by a valley-projected periodic Hamiltonian that accounts for position-dependent stacking. We focus below on the case of twisted bilayer graphene (TBG) sandwiched by aligned hexagonal Boron Nitride (hBN) layers.

Orbital Magnetization of MATBG on Hexagonal Boron Nitride—The contribution to the orbital magnetization of 2D Bloch electrons from a single band is[7, 15, 16]

$$M^n(\mu) = \int \frac{d^2\mathbf{k}}{(2\pi)^2} \mathcal{M}^n(\mathbf{k}, \mu) f(\mu - \varepsilon_n(\mathbf{k})) \quad (3)$$

$$\mathcal{M}^n(\mathbf{k}, \mu) = \frac{e}{\hbar} \text{Im} \sum_{n' \neq n} \frac{\langle n | \partial_x H | n' \rangle \langle n' | \partial_y H | n \rangle}{(\varepsilon_n - \varepsilon_{n'})^2} (\varepsilon_n + \varepsilon_{n'} - 2\mu)$$

where n is a band index, μ is the chemical potential, $f(\mu - \varepsilon_n(\mathbf{k}))$ is Fermi-Dirac distribution and $\partial_j H = \partial H / \partial k_j$ is the velocity operator. In Eq. (3) $|n\rangle$ is a Bloch state whose wave vector dependence is left implicit. We separate the orbital magnetization in Eq. (3) into two parts, $M^n(\mu) = M_1^n(\mu) + M_2^n(\mu)$, where $M_2^n(\mu)$ selects the contribution that is explicitly proportional to μ . When the band is full

$$M_1^n(\mu) = \frac{e}{\hbar} \text{Im} \sum_{n' \neq n} \int \frac{d^2\mathbf{k}}{(2\pi)^2} \frac{\langle n | \partial_x H | n' \rangle \langle n' | \partial_y H | n \rangle}{(\varepsilon_n - \varepsilon_{n'})^2} (\varepsilon_n + \varepsilon_{n'}) \quad (4)$$

is independent of μ , whereas

$$M_2^n(\mu) = \frac{e}{\hbar} \text{Im} \sum_{n' \neq n} \int \frac{d^2\mathbf{k}}{(2\pi)^2} \frac{\langle n | \partial_x H | n' \rangle \langle n' | \partial_y H | n \rangle}{(\varepsilon_n - \varepsilon_{n'})^2} (-2\mu) \quad (5)$$

includes the edge state contribution and is proportional to μ with proportionality constant $C_n e / (2\pi\hbar)$, where C_n is Chern number of band n .

We now apply these expressions to TBG encapsulated between hBN layers whose influence on the low-energy graphene Hamiltonian is captured[17–21] in part by a mass m term representing the spatially averaged difference between carbon π -orbital energies on different honeycomb sublattices. The valley-projected twisted graphene bilayer Hamiltonian $\mathcal{H}(\mathbf{r}) = h_0^{(1)} + h_0^{(2)} + T(\mathbf{r}) + h.c.$, where $h_0^{(l)}(\mathbf{r}) = -i\partial_x \sigma_x - i\partial_y \sigma_y + m_l \sigma_z$ is the massive Dirac Hamiltonian of layer l , σ acts on the sublattice degrees of freedom, and $T(\mathbf{r})$ is the periodic interlayer tunneling Hamiltonian[14]. The conclusions we reach below rest in part on a particle-hole symmetry property of this Hamiltonian, discussed at greater length in supplementary material (SM) S1.

$$\tau_z \sigma_x \mathcal{H}(x, y) \sigma_x \tau_z = -\mathcal{H}(-x + d, y) \quad (6)$$

$$\tau_x \mathcal{H}(x, y) \tau_x = \mathcal{H}^*(-x + d, y) \quad (7)$$

In Eqs. (6,7), τ acts on the layer degrees of freedom and $d = a_M / \sqrt{3}$ (modulo $\sqrt{3}a_M$) where a_M is moiré lattice constant. Symmetry (6) states that up to a translation and a change in the sign of the interlayer tunneling term, sublattice exchange combined with reflection by the y -axis simply changes the sign of the Hamiltonian. Eq. (6) becomes exact in the limit of small twist angles and is accurate in MATBG. Eq. (7) is satisfied only when the masses of two graphene layers are identical $m_1 = m_2$. In momentum space, the Hamiltonian satisfies

$$\tau_z \sigma_x H(k_x, k_y) \sigma_x \tau_z = -H(-k_x, k_y) \quad (8)$$

$$\tau_x H(k_x, k_y) \tau_x = H^*(k_x, -k_y) \quad (9)$$

Given Eq. (8), as detailed in SM S1, it can be shown that the contribution to the orbital magnetization from a valley vanishes when the chemical potential lies in the middle of the gap between its conduction and valence bands.

For graphene on hBN m decreases with relative twist angle, has been estimated using DFT[19, 20] to be ~ 3.62 meV for perfect alignment, and can be substantially enhanced by interaction effects absent in DFT. The experimental m for nearly aligned graphene on hBN is $\sim 10 - 15$ meV[22, 23]. Figure 1 illustrates the K valley low energy moiré band dispersions and Chern numbers of 1.1° -TBG for different mass choices: (a) $m_1 = m_2 = 10$ meV, (b) $m_1 = 10, m_2 = 0$ meV and (c) $m_1 = -m_2 = 10$ meV. The choice $m_1 = m_2$ corresponds to the case in which both graphene layers are aligned and have equivalent stacking orientation with respect to hBN, while $m_1 = -m_2$ corresponds to the case in which both graphene layers are aligned but have the opposite stacking orientations with respect to hBN. The choice $m_l = 0$ corresponds to layer l having

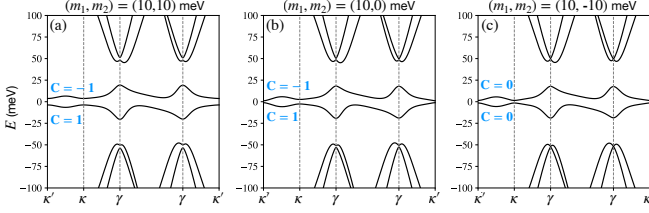


FIG. 1. 1.1° valley-K TBG moiré band structures for three hBN-induced mass choices. (a) $m_1 = m_2 = 10$ meV produces a band gap $E_g^0 \sim 7.5$ meV at charge neutrality. The flat bands are non-trivial with Chern numbers $C = \pm 1$. (b) $m_1 = 10, m_2 = 0$ meV produces a band gap $E_g^0 \sim 2.3$ meV. The flat bands are again non-trivial with Chern numbers $C = \pm 1$. (c) $m_1 = -m_2 = -10$ meV produces a band gap $E_g^0 \sim 3$ meV with topologically trivial valley-projected flat bands. The moiré bands were calculated using a low-energy continuum model[14] with interlayer tunneling strength $w^{AB} = 110$ meV and $w^{AA}/w^{AB} = 0.85$ to account for corrugation and strain.

a large misalignment relative to hBN so that strain enhancement is absent. We find that gaps (E_g^0) appear at charge neutrality, that the bands are relatively flat for twists near the magic angle, and that they have non-zero Chern numbers when both layers have the same alignment or only one layer is aligned. The case of opposite masses always produces trivial bands (Fig. 1(c)). In all three cases sublattice-symmetry breaking gaps the Dirac points at the moiré Brillouin zone (MBZ) corners that otherwise link the conduction and valence bands. For convenience we focus below on the case of Fig. 1(a).

Spin and Valley—When the spin/valley degeneracy of the moiré flat bands is maintained (Fig. 2(a)), gaps appear only when the number of electrons per moiré flat band is a multiple of four. In mean-field theory gaps at odd integer numbers of electrons per period can be achieved only if the quasiparticle bands are modified by both spontaneous spin-splitting Δ_s and spontaneous valley splitting Δ_v . For three electrons per moiré period, the density at which the QAHE has been observed, all the majority spin's flat bands are occupied and the magnetization contributions from its two valleys cancel. In order to have a gap at three electrons per moiré period, both Δ_v and Δ_s must be larger than the flat conduction band width w (Fig. 2(b)), a condition that is easily achievable near magic angle orientations because w is extremely small. For large enough spin splitting, $\Delta_s > w + E_g^0$, we can consider only the four minority spin bands illustrated schematically in Fig. 2(c-d). E_g^0 is the band gap at charge neutrality for a valley-projected Hamiltonian. The highest energy flat band is then the conduction band of the minority valley and the second highest band, which is not fully occupied when the insulator is hole doped, can either be the conduction band of the majority valley (Fig. 2(c)) or the valence band of the minority valley (Fig. 2(d)). For moderate spin splitting (Fig. 2(e-f)), $w < \Delta_s < w + E_g^0$, the majority spins can play a role when the insulator is hole doped. The second highest band is either the conduction band of the minority spin majority valley (Fig. 2(e)) or the conduction band of the minority valley with majority spin (Fig. 2(f)).

Given Δ_s and Δ_v and a total moiré filling factor, the total

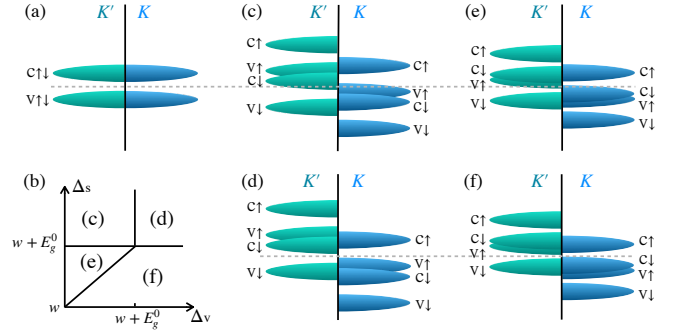


FIG. 2. (a) Each flat band is four-fold degenerate in the absence of interactions. (b) Band configurations depending on valley Δ_v , and spin Δ_s splittings. w is the flat band bandwidth and E_g^0 is the gap between conduction and valence for a given spin/valley. (c-f) Schematically illustrate the valley- and spin-polarized bands in different (Δ_s, Δ_v) regimes. (c) $w < \Delta_v < w + E_g^0 < \Delta_s$; (d) $\Delta_v, \Delta_s > w + E_g^0$; (e) $w < \Delta_v < \Delta_s < w + E_g^0$; (f) $w < \Delta_s < w + E_g^0, \Delta_s < \Delta_v$.

orbital magnetization is calculated by summing Eq. (3) over spin/valley flavors. Figure 3(a) plots the single-flavor contribution (solid line) from valleys K and K' at twist angle 1.1° as a function of chemical potential μ measured relative to the mid-point between its shifted conduction and valence bands. As explained previously the magnetization contribution from each valley vanishes at mid-gap and varies linearly within the gap. Because valleys K and K' are time-reversed counterparts, their magnetization contributions are opposite in sign. The dotted and dash-dotted lines in Fig. 3(a) separate the M_1 and M_2 contributions defined in Eq. (4) and (5). The chemical potential μ range plotted in Fig. 3(a) covers from the flat valence band bottom to the flat conduction band top[24]. Figure 3(b) plots the total magnetization from two minority spin valleys that are split by $\Delta_v = 19.5$ meV, larger than the bandwidth but smaller than the sum of bandwidth and the band gap, corresponding to the situation illustrated in Fig. 2(c). Note that in this case the total magnetization's sign does switch when μ crosses the gap highlighted by grey stripes in Fig. 3(b). Assuming that the broken TR state at $3/4$ filling of the conduction bands has unpolarized valleys for majority spins and valley polarization for minority spins, the magnetization for weak n -doping of the insulator is $M_{c,t}^K + M_{c,b}^{K'} = M_{c,t}^K - M_{c,b}^K \equiv M^+ < 0$ [25], as seen in Fig. 3(a). Here c specifies the flat conduction band and b and t specify whether the chemical potential is placed at the bottom or top band extremum. The magnetization changes sign across the gap whenever $|\Delta M|$ exceeds $|M^+|$ and M^+ has the same sign as the Chern number of occupied bands. Necessary conditions for a difference in sign between the magnetization at weak n and p doping are discussed in more detail in SM S2. In Fig. 4(a-b) we plot the magnetization as a function of valley splitting Δ_v and band filling factor for 1.1° -TBG for: (a) $\Delta_s = 23$ meV, corresponding to Fig. 2(c-d) ($\Delta_s > w + E_g^0$) and (b) $\Delta_s = 16$ meV, corresponding to Fig. 2(e-f) ($w < \Delta_s < w + E_g^0$). ($w \approx 15.5$ meV for 1.1° TBG.) For both cases, the magnetization changes sign near $3/4$ filling, with the sign change occurring at a filling factor slightly

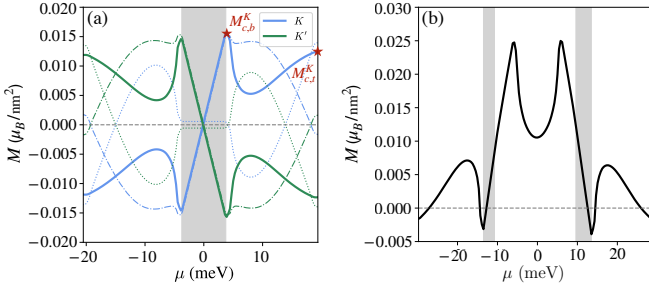


FIG. 3. Single flavor orbital magnetization of 1.1° -TBG. The grey stripes indicate the band gap. (a) Single-valley magnetization M (solid line), and M_1 (dotted) and M_2 (dash-dotted) contributions, for valleys K (blue) and K' (green) as a function of chemical potential μ relative to gap center. (b) Total minority spin magnetization summing two valleys when $\Delta_v = 19.5$ meV and Δ_s is very large, corresponding to the situation illustrated in Fig. 2(c).

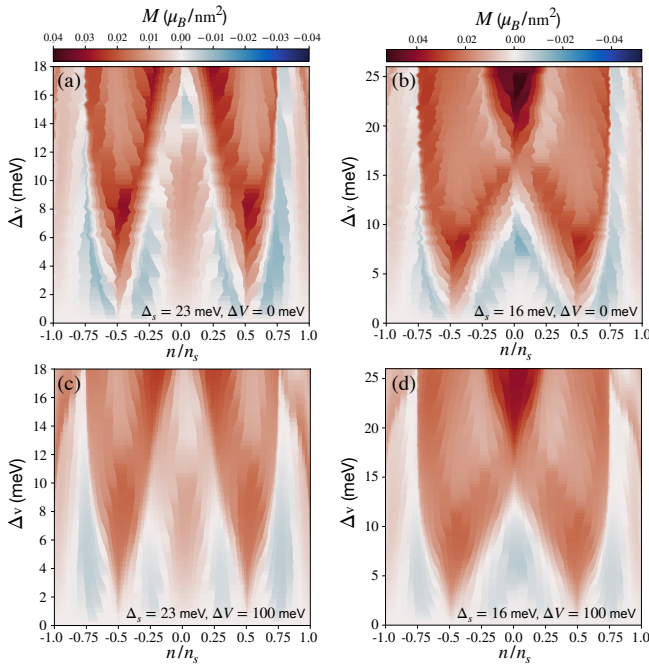


FIG. 4. Magnetization as a function of valley splitting Δ_v and filling factor n/n_s for a fixed spin splitting Δ_s for 1.1° -TBG. (a) $\Delta_s = 23$ meV, larger than the sum of flat band bandwidth w and the band gap $E_g^0 \sim 7.5$ meV, corresponding to cases in Fig. 2(c-d). (b) $\Delta_s = 16$ meV, larger than w but smaller than $w + E_g^0$, corresponding to cases in Fig. 2(e-f). (c-d) Same parameters as (a-b) but with on-site energy difference $\Delta V = 100$ meV between two graphene layers.

smaller than $3/4$ for $\Delta_v < w$. Magnetization sign changes with doping can therefore occur whether or not Δ_v is large enough to open a gap at three quarters filling. Figures 4(c-d) illustrate the effect of gate voltage by setting the interlayer on-site energy difference to $\Delta V = V_1 - V_2 = 100$ meV. We see that large gate voltage distort the flat bands, making the bandwidth larger and band the gap smaller, thereby suppressing magnetization sign-switching effect as shown in Fig. 4(c-d). (The influence of large gate voltages on the single-valley magnetization is illustrated in Fig. 7 of the SM.)

Discussion—Chern insulators are two-dimensional electron systems with charge gaps and QAHE, and have now been realized experimentally by two distinct mechanisms. In magnetized topological insulators[1, 26–31], the QAHE is driven by the exchange interactions between spin-local-moments that order ferromagnetically and two Dirac-cones localized on opposite surfaces of a topological insulator thin film. In bilayer graphene, on the other hand, the QAHE is driven by broken sublattice symmetry, which gaps Dirac cones and induces Berry curvatures of opposite signs near TR-partner valleys, combined with TR symmetry breaking via condensation of electrons into one of the two valleys. Both of these mechanisms differ from the one identified in the original theoretical work of Haldane[6] in which the QAHE is driven by broken TR symmetry that leads to Berry curvatures of the same sign near opposite valleys.

In twisted graphene bilayers sublattice polarization can be enforced by alignment with a hBN layer, and spontaneous valley polarization is energetically preferred when the moiré bands are narrowed by tuning the orientation close to the magic twist angle. Because the TR symmetry breaking mechanism is orbital, the spontaneous magnetization associated with the MATBG QAHE state is dominantly orbital. We have shown in this paper that this unusual circumstance changes the considerations[32] that normally limit our ability to control magnetic states electrically. The most extreme example of the strong electrical effects that are possible in orbital Chern insulators is a consequence of the jump in magnetization between weak n -doping and weak p -doping produced by gap edge states. We have shown in this paper that the sign of magnetization, and therefore the thermodynamically preferred sense of TR breaking in a weak magnetic field as characterized for example by valley polarization or anomalous Hall effect sign, can be changed by electrostatic doping. This property could be of technological value if other examples of orbital Chern insulators, which have higher transition temperatures, are discovered in the future. When the sign of the magnetization is independent of carrier density, the Streda[33] formula implies that magnetic-switching between quantum anomalous Hall states will be more robust for either n - or p -doping, depending on the relative sign of the magnetization and the Hall conductivity. This behavior is common in current experiments[3, 4, 13, 34, 35]. Anomalous-Hall switching that is equally robust for n - and p -doping therefore signals the magnetization sign switch that we expect to be common in large gap orbital Chern insulators. Detailed illustrations are in the SM S3.

Acknowledgements—JJS and AHM thank SDH for stimulating discussions. AHM was supported by DOE grant FG02-02ER45958. JZ was supported by the National Science Foundation through the Center for Dynamics and Control of Materials: an NSF MRSEC under Cooperative Agreement No. DMR-1720595. The authors acknowledge the Texas Advanced Computing Center (TACC) at The University of Texas at Austin for providing HPC resources that have contributed to the research results reported within this paper.

-
- [1] C.-Z. Chang, J. Zhang, X. Feng, J. Shen, Z. Zhang, M. Guo, K. Li, Y. Ou, P. Wei, L.-L. Wang, Z.-Q. Ji, Y. Feng, S. Ji, X. Chen, J. Jia, X. Dai, Z. Fang, S.-C. Zhang, K. He, Y. Wang, L. Lu, X.-C. Ma, and Q.-K. Xue, *Science* **340**, 167 (2013).
- [2] A. L. Sharpe, E. J. Fox, A. W. Barnard, J. Finney, K. Watanabe, T. Taniguchi, M. A. Kastner, and D. Goldhaber-Gordon, *Science* **365**, 605 (2019).
- [3] G. Chen, A. L. Sharpe, E. J. Fox, Y.-H. Zhang, S. Wang, L. Jiang, B. Lyu, H. Li, K. Watanabe, T. Taniguchi, Z. Shi, T. Senthil, D. Goldhaber-Gordon, Y. Zhang, and F. Wang, arXiv:1905.06535.
- [4] M. Serlin, C. L. Tschirhart, H. Polshyn, Y. Zhang, J. Zhu, K. Watanabe, T. Taniguchi, L. Balents, and A. F. Young, *Science* (2019), 10.1126/science.aay5533.
- [5] D. J. Thouless, M. Kohmoto, M. P. Nightingale, and M. den Nijs, *Phys. Rev. Lett.* **49**, 405 (1982).
- [6] F. D. M. Haldane, *Phys. Rev. Lett.* **61**, 2015 (1988).
- [7] D. Xiao, M.-C. Chang, and Q. Niu, *Rev. Mod. Phys.* **82**, 1959 (2010).
- [8] A. MacDonald, arXiv:cond-mat/9410047.
- [9] F. London, *Phys. Rev.* **74**, 562 (1948).
- [10] J. Jung, M. Polini, and A. H. MacDonald, *Phys. Rev. B* **91**, 155423 (2015).
- [11] H. C. Po, L. Zou, T. Senthil, and A. Vishwanath, *Phys. Rev. B* **99**, 195455 (2019).
- [12] Z. Song, Z. Wang, W. Shi, G. Li, C. Fang, and B. A. Bernevig, *Phys. Rev. Lett.* **123**, 036401 (2019).
- [13] X. Lu, P. Stepanov, W. Yang, M. Xie, M. A. Aamir, I. Das, C. Urgell, K. Watanabe, T. Taniguchi, G. Zhang, A. Bachtold, A. H. MacDonald, and D. K. Efetov, *Nature* **574**, 653 (2019).
- [14] R. Bistritzer and A. H. MacDonald, *Proceedings of the National Academy of Sciences* **108**, 12233 (2011).
- [15] T. Thonhauser, D. Ceresoli, D. Vanderbilt, and R. Resta, *Phys. Rev. Lett.* **95**, 137205 (2005).
- [16] D. Ceresoli, T. Thonhauser, D. Vanderbilt, and R. Resta, *Phys. Rev. B* **74**, 024408 (2006).
- [17] J. R. Wallbank, A. A. Patel, M. Mucha-Kruczyński, A. K. Geim, and V. I. Fal'ko, *Phys. Rev. B* **87**, 245408 (2013).
- [18] P. Moon and M. Koshino, *Phys. Rev. B* **90**, 155406 (2014).
- [19] J. Jung, A. M. DaSilva, A. H. MacDonald, and S. Adam, *Nature Communications* **6**, 6308 (2015).
- [20] J. Jung, E. Laksono, A. M. DaSilva, A. H. MacDonald, M. Mucha-Kruczyński, and S. Adam, *Phys. Rev. B* **96**, 085442 (2017).
- [21] M. Kindermann, B. Uchoa, and D. L. Miller, *Phys. Rev. B* **86**, 115415 (2012).
- [22] B. Hunt, J. D. Sanchez-Yamagishi, A. F. Young, M. Yankowitz, B. J. LeRoy, K. Watanabe, T. Taniguchi, P. Moon, M. Koshino, P. Jarillo-Herrero, and R. C. Ashoori, *Science* **340**, 1427 (2013).
- [23] N. R. Finney, M. Yankowitz, L. Muraleetharan, K. Watanabe, T. Taniguchi, C. R. Dean, and J. Hone, *Nature Nanotechnology* (2019), 10.1038/s41565-019-0547-2.
- [24] Note that M_2 (dash-dotted line) should vanish when the flat bands are completely filled or completely empty because the total Chern number of all occupied bands is zero in both cases; the numerical error in Fig. 3(a) is difficult to completely eliminate because small inaccuracies in the Berry curvature integrals are magnified when multiplied by the chemical potential μ .
- [25] Here we assume valley K' is split up and valley K is split down. The sign of M^+ depends on how valleys split.
- [26] J. G. Checkelsky, R. Yoshimi, A. Tsukazaki, K. S. Takahashi, Y. Kozuka, J. Falson, M. Kawasaki, and Y. Tokura, *Nature Physics* **10**, 731 (2014).
- [27] X. Kou, S.-T. Guo, Y. Fan, L. Pan, M. Lang, Y. Jiang, Q. Shao, T. Nie, K. Murata, J. Tang, Y. Wang, L. He, T.-K. Lee, W.-L. Lee, and K. L. Wang, *Phys. Rev. Lett.* **113**, 137201 (2014).
- [28] A. J. Bestwick, E. J. Fox, X. Kou, L. Pan, K. L. Wang, and D. Goldhaber-Gordon, *Phys. Rev. Lett.* **114**, 187201 (2015).
- [29] C.-Z. Chang, W. Zhao, D. Y. Kim, H. Zhang, B. A. Assaf, D. Heiman, S.-C. Zhang, C. Liu, M. H. W. Chan, and J. S. Moodera, *Nature Materials* **14**, 473 (2015).
- [30] M. Mogi, R. Yoshimi, A. Tsukazaki, K. Yasuda, Y. Kozuka, K. S. Takahashi, M. Kawasaki, and Y. Tokura, *Applied Physics Letters* **107**, 182401 (2015).
- [31] J. Jiang, D. Xiao, F. Wang, J.-H. Shin, D. Andreoli, J. Zhang, R. Xiao, Y.-F. Zhao, M. Kayyalha, L. Zhang, K. Wang, J. Zang, C. Liu, N. Samarth, M. H. W. Chan, and C.-Z. Chang, arXiv:1901.07611.
- [32] B. Dieny and M. Chshiev, *Rev. Mod. Phys.* **89**, 025008 (2017).
- [33] P. Streda, *Journal of Physics C: Solid State Physics* **15**, L717 (1982).
- [34] L. Wang, E.-M. Shih, A. Ghiotto, L. Xian, D. A. Rhodes, C. Tan, M. Claassen, D. M. Kennes, Y. Bai, B. Kim, K. Watanabe, T. Taniguchi, X. Zhu, J. Hone, A. Rubio, A. Pasupathy, and C. R. Dean, arXiv:1910.12147.
- [35] P. Stepanov, I. Das, X. Lu, A. Fahimniya, K. Watanabe, T. Taniguchi, F. H. L. Koppens, J. Lischner, L. Levitov, and D. K. Efetov, arXiv:1911.09198.

**SUPPLEMENTAL MATERIAL:
THE CURIOUS MAGNETIC PROPERTIES OF ORBITAL CHERN INSULATORS**

S1. SYMMETRY ANALYSIS

Below we prove that the moiré Hamiltonian $\mathcal{H}(\mathbf{r})$ of TBG on hBN substrates has the following symmetry properties:

$$\tau_z \sigma_x \mathcal{H}(x, y) \sigma_x \tau_z = -\mathcal{H}(-x + d, y) \quad (10)$$

$$\tau_x \mathcal{H}(x, y) \tau_x = \mathcal{H}^*(-x + d, y) \quad (11)$$

The first of these properties applies only in the limit of small twist angles and the second only if the Dirac masses m_1 and m_2 in the two layers are identical. The Pauli matrices σ and τ act on sublattice and layer degrees of freedom respectively.

The moiré Hamiltonian

$$\mathcal{H}(\mathbf{r}) = \begin{pmatrix} h_0^{(1)}(\mathbf{r}) & T(\mathbf{r}) \\ T^\dagger(\mathbf{r}) & h_0^{(2)}(\mathbf{r}) \end{pmatrix} \quad (12)$$

$T(\mathbf{r})$ is the interlayer tunneling matrices and superscripts (1) and (2) denote graphene layers. $h_0(\mathbf{r})$ is the massive Dirac Hamiltonian

$$h_0(x, y) = -i\partial_x \sigma_x - i\partial_y \sigma_y + m\sigma_z \quad (13)$$

and we have

$$\sigma_x h_0(x, y) \sigma_x = -h_0(-x, y) \quad (14)$$

For the interlayer tunneling term,

$$T(\mathbf{r}) = w_0 \sum_{j=1}^3 e^{-i\mathbf{q}_j \cdot \mathbf{r}} T_j \quad (15)$$

where $\mathbf{q}_1 = (0, -1)$, $\mathbf{q}_2 = (\sqrt{3}/2, 1/2)$, $\mathbf{q}_3 = (-\sqrt{3}/2, 1/2)$ (in units of $4\pi/3a_M$) are three momentum boosts. a_M is the moiré lattice constant. $w_0 = 110$ meV is the tunneling strength, and

$$T_1 = \begin{pmatrix} 1 & 1 \\ 1 & 1 \end{pmatrix}, \quad T_2 = \begin{pmatrix} e^{-i\phi} & 1 \\ e^{i\phi} & e^{-i\phi} \end{pmatrix}, \quad T_3 = \begin{pmatrix} e^{i\phi} & 1 \\ e^{-i\phi} & e^{i\phi} \end{pmatrix} \quad (16)$$

with $\phi = 2\pi/3$. Substituting \mathbf{q}_j and T_j in Eq. (15),

$$T(-x + d, y) = e^{-i\mathbf{q}_1 \cdot \mathbf{r}} \sigma_x T_1 \sigma_x + e^{-i\mathbf{q}_2 \cdot \mathbf{r}} e^{i(2\phi + q_{2x}d)} \sigma_x T_2 \sigma_x + e^{-i\mathbf{q}_3 \cdot \mathbf{r}} e^{i(\phi - q_{3x}d)} \sigma_x T_3 \sigma_x \quad (17)$$

$$\sigma_x T(x, y) \sigma_x = e^{-i\mathbf{q}_1 \cdot \mathbf{r}} \sigma_x T_1 \sigma_x + e^{-i\mathbf{q}_2 \cdot \mathbf{r}} \sigma_x T_2 \sigma_x + e^{-i\mathbf{q}_3 \cdot \mathbf{r}} \sigma_x T_3 \sigma_x \quad (18)$$

and we get

$$\sigma_x T(x, y) \sigma_x = T(-x + d, y) \quad (19)$$

where $d = a_M/\sqrt{3}$ modulo $\sqrt{3}a_M$. In other words sublattice-exchange of the tunneling Hamiltonian is equivalent to reflection by the y -axis combined with a translation. Combining Eq. (14) and (19), we obtain

$$\tau_z \sigma_x \mathcal{H}(x, y) \sigma_x \tau_z = -\mathcal{H}(-x + d, y) \quad (20)$$

Similarly,

$$T^\dagger(x, y) = e^{i\mathbf{q}_1 \cdot \mathbf{r}} T_1 + e^{i\mathbf{q}_2 \cdot \mathbf{r}} e^{-i\phi} T_2 + e^{i\mathbf{q}_3 \cdot \mathbf{r}} e^{i\phi} T_3 \quad (21)$$

$$T^*(-x + d, y) = e^{i\mathbf{q}_1 \cdot \mathbf{r}} T_1 + e^{i\mathbf{q}_2 \cdot \mathbf{r}} e^{-iq_{2x}d} T_2 + e^{i\mathbf{q}_3 \cdot \mathbf{r}} e^{iq_{3x}d} T_3 \quad (22)$$

$$T^\dagger(x, y) = T^*(-x + d, y) \quad (23)$$

$d = a_M/\sqrt{3}$. If $m_1 = m_2$, then

$$\tau_x \mathcal{H}(x, y) \tau_x = \mathcal{H}^*(-x + d, y) \quad (24)$$

Applying Bloch's theorem to Eq. (10,11), we see that $H(\mathbf{k})$ satisfies

$$\tau_z \sigma_x H(k_x, k_y) \sigma_x \tau_z = -H(-k_x, k_y) \quad (25)$$

$$\tau_x H(k_x, k_y) \tau_x = H^*(k_x, -k_y) \quad (26)$$

As a result of Eq. (25), the eigenvalues and eigenvectors satisfy $\varepsilon_{c_i}(k_x, k_y) = -\varepsilon_{v_i}(-k_x, k_y)$, $\psi_{c_i}(k_x, k_y) = \tau_z \sigma_x \psi_{v_i}(-k_x, k_y)$. Here $i = 1, 2, \dots$ labels the i -th conduction (c_i) or valence (v_i) band counting from charge neutrality. For Eq. (26), $\varepsilon_n(k_x, k_y) = \varepsilon_n(k_x, -k_y)$, $\psi_n(k_x, k_y) = \tau_x \psi_n^*(k_x, -k_y)$, where n label bands.

Now let us define the orbital magnetization contribution due to mixing between bands n and n' :

$$\mathfrak{M}^{nn'} = \frac{e}{\hbar} \text{Im} \int_{\text{MBZ}} \frac{d^2 \mathbf{k}}{(2\pi)^2} \frac{\langle n | \partial_x H | n' \rangle \langle n' | \partial_y H | n \rangle}{(\varepsilon_n - \varepsilon_{n'})^2} (\varepsilon_n + \varepsilon_{n'}) \quad (27)$$

When the chemical potential at neutrality is in the middle of the gap, and the Hamiltonian has been truncated to a finite number ($2N$) of bands via a plane-wave expansion cut-off, the total orbital magnetization is

$$\begin{aligned} \sum_{i=1}^N M^{v_i} &= \sum_{i,j=1, i \neq j}^N \mathfrak{M}^{v_i v_j} + \sum_{i,j=1}^N \mathfrak{M}^{v_i c_j} \\ &= \sum_{i,j=1, i \neq j}^N \mathfrak{M}^{v_i v_j} + \sum_{i=1}^N \mathfrak{M}^{v_i c_i} + \sum_{i,j=1, i \neq j}^N \mathfrak{M}^{v_i c_j} \end{aligned} \quad (28)$$

The first term in the last expression of Eq. (28) is zero because $\mathfrak{M}^{v_i v_i} + \mathfrak{M}^{v_i v_j} = 0$. The second term in the last expression of Eq. (28) is also zero because $\varepsilon_{c_i} + \varepsilon_{v_i}$ is antisymmetric and $\text{Im} \langle \psi_{v_i} | \partial_x H | \psi_{c_i} \rangle \langle \psi_{c_i} | \partial_y H | \psi_{v_i} \rangle$ is symmetric when k_x is reflected to $-k_x$. Similarly, we can also prove that $\mathfrak{M}^{v_j c_i} + \mathfrak{M}^{v_i c_j} = 0$. It follows that the total magnetization at mid-gap vanishes.

S2. ELECTRICAL REVERSAL OF MAGNETIZATION SIGN AT 1/4 AND 3/4 FILLING

Here we elaborate on how the orbital magnetization changes as the chemical potential or filling is tuned across the band gap. As shown in Fig. 5, when the filling is just above 3/4, that is when the chemical potential is at μ_1 , the orbital magnetization is

$$M_{3/4}^+ = M_{c,t}^K + M_{c,b}^{K'} = M_{c,t}^K - M_{c,b}^K \quad (29)$$

When the filling is just below 3/4, that is at $\mu = \mu_2$, the only change in orbital magnetization is δM across the band gap $\Delta_g^{3/4}$:

$$M_{3/4}^- = M_{c,t}^K - M_{c,b}^K - \frac{Ce}{2\pi\hbar} \Delta_g^{3/4} \quad (30)$$

where $\Delta_g^{3/4}$ is the size of band gap at $n/n_s = 3/4$ and C is the total Chern number of occupied bands. $C = -1$ in the example shown in Fig. 5 in which valley K energy bands are lower than valley K' . (For the opposite sense of sublattice polarization, that is opposite sign in mass terms, the sense of the relationship between Chern number and valley is reversed.) If $M_{c,t}^K - M_{c,b}^K < 0$, as we argued in the main text, and the band gap $\Delta_g^{3/4}$ is large enough, M reverses the sign as the chemical potential is tuned from μ_2 to μ_1 . The measured activation gap at $n/n_s = 3/4$ is ~ 2 meV[4], corresponding to $\delta M = M(\mu_2) - M(\mu_1) \approx 0.008 \mu_B/\text{nm}^2$. In our calculations, $M_{c,t}^K - M_{c,b}^K \sim -0.003 \mu_B/\text{nm}^2$ for MATBG with broken sublattice symmetry. As shown in Fig. 6, $M_{c,b}^K - M_{c,t}^K$ is typically larger for larger band gap at charge neutrality and smaller twist angle.

At 1/4 filling, the analysis is complicated because the magnetization switching property is dependent on how strongly the valleys split, how large the conduction-valence splitting is, and how flat the bands are. Fig. 5 illustrates four different valley and spin splitting cases. For large conduction-valence band gaps and small spin splitting, corresponding to Fig. 5(a), the magnetization at $\mu = \mu_3$ is

$$M_{1/4}^+ = 2M_{c,b}^{K'} + M_{c,t}^K + M_{c,b}^K + \frac{e\Delta_v}{2\pi\hbar} \quad (31)$$

$$= M_{c,t}^K - M_{c,b}^K + \frac{e\Delta_v}{2\pi\hbar} \quad (32)$$

and at $\mu = \mu_4$,

$$M_{1/4}^- = M_{1/4}^+ + \frac{e\Delta_g^{1/4}}{2\pi\hbar} \quad (33)$$

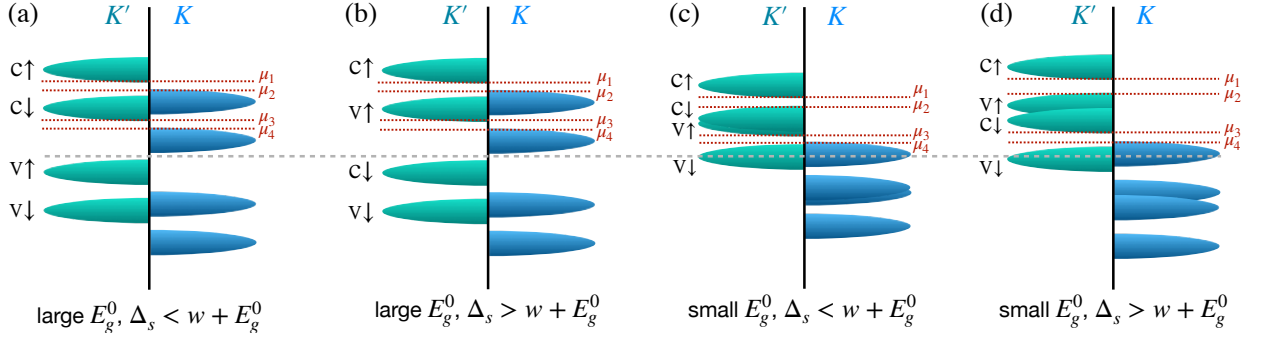


FIG. 5. Four cases of conduction-valence band splitting E_g^0 and spin splitting Δ_s which realize different situations at $1/4$ filling. Typically the magnetization will reverse its sign for case (b).

Whether the orbital magnetization can be reversed or not at $n/n_s = 1/4$ depends on $M_{c,t}^K - M_{c,b}^K$, valley splitting Δ_v and the activation gap $\Delta_g^{1/4}$. Since $e\Delta_v/2\pi\hbar$ is typically larger than $|M_{c,t}^K - M_{c,b}^K|$, magnetization sign reversal across the gap may be uncommon at $n/n_s = 1/4$. For large band gaps and large spin splitting, corresponding to Fig. 5(b), all majority spin bands are occupied, thus only minority spin bands need to be considered. The situation at $1/4$ filling is similar to that of $3/4$ filling.

For small band gap and small spin splitting, corresponding to Fig. 5(c), the magnetization at μ_3 is

$$M_{1/4}^+ = M_{v,b}^{K'} + M_{c,t}^K + M_{c,b}^{K'} + \frac{e(w + E_g^0 - \Delta_s)}{2\pi\hbar} + M_{c,t}^K \quad (34)$$

$$= 3M_{c,t}^K - M_{c,b}^K + \frac{e(w + E_g^0 - \Delta_s)}{2\pi\hbar} \quad (35)$$

and at μ_4 ,

$$M_{1/4}^- = M_{1/4}^+ + \frac{e\Delta_g^{1/4}}{2\pi\hbar} \quad (36)$$

For small band gap and large spin splitting, corresponding to Fig. 5(d),

$$M_{1/4}^+ = M_{v,b}^{K'} + M_{c,t}^K + M_{c,b}^{K'} + M_{c,t}^K = 3M_{c,t}^K - M_{c,b}^K \quad (37)$$

$$M_{1/4}^- = M_{1/4}^+ + \frac{e\Delta_g^{1/4}}{2\pi\hbar} \quad (38)$$

Since $3M_{c,t}^K - M_{c,b}^K$ is typically positive, it is uncommon to reverse the magnetization across the gap at the quarter filling. The only possible case corresponds to Fig. 5(b).

Our single-particle model is identically applicable to the negative filling side. Nevertheless, absence of observing the anomalous Hall effect on the hole side is still an open question and is out of the scope of this paper.

S3. INDICATION OF MAGNETIZATION SIGN SWITCH IN LANDAU FAN

When the sign of the magnetization across the band gap is independent of carrier density n , the quantum anomalous Hall states will be more robust for either n - or p -doping, depending on the relative sign of the magnetization and the Hall conductivity. There are two possible cases as shown in top figures of Fig. 8(a,b), the magnetization M has the same sign (Fig. 8(a)) as or the opposite sign (Fig. 8(b)) to the Hall conductivity. Assume positive magnetic field B favors positive magnetization, then the quantum anomalous Hall state in case Fig. 8(a) will be more robust for n -doping and in case Fig. 8(b) will be more robust for p -doping. Therefore we can only observe Landau fans on one side of carrier density.

If the sign of the magnetization switches across the band gap, the quantum anomalous Hall states will be equally robust for n - and p -doping, as illustrated in Fig. 8(c). For a specific magnetic field direction, Landau fans with opposite Chern numbers on both sides of carrier density are observable.

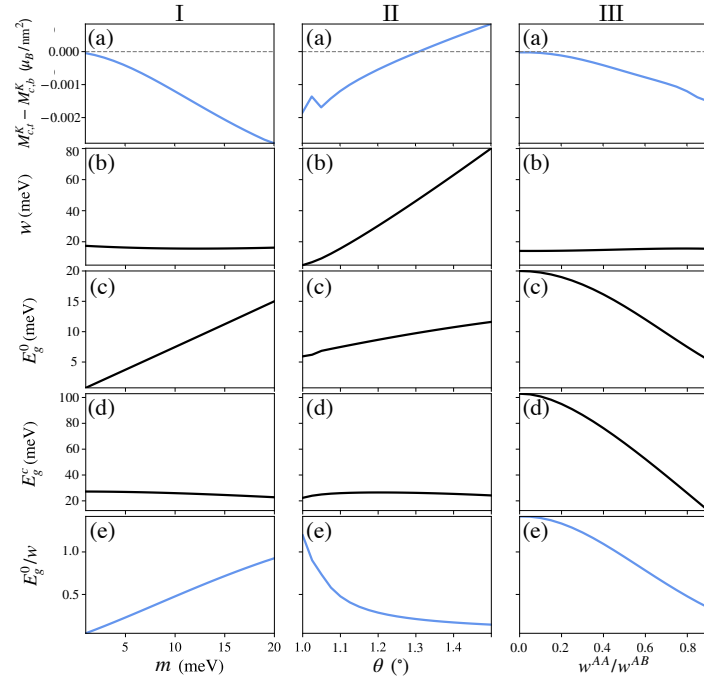


FIG. 6. Each row shares the same y-axis and each column shares the same x-axis. Rows (a-e) represent (a) $M_{c,t}^K - M_{c,b}^K$, (b) the flat band bandwidth w , (c) valley-projected band gap at charge neutrality E_g^0 , (d) valley-projected band gap between the flat band and the nearest remote band E_g^c and (e) the ratio E_g^0/w as y-axes. Columns (I-III) represent (I) the average mass $m_1 = m_2 = m$, (II) twist angle θ and (III) the ratio of interlayer tunneling matrix elements' magnitude w^{AA}/w^{AB} as x-axes. (I) is at $\theta = 1.1^\circ$ and $w^{AA}/w^{AB} = 0.8$; (II) is at $m = 10$ meV and $w^{AA}/w^{AB} = 0.8$; (III) is at $\theta = 1.1^\circ$ and $m = 10$ meV.

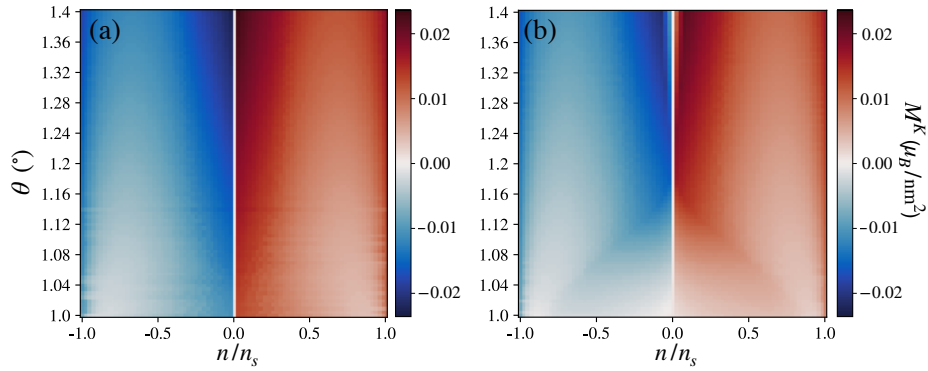


FIG. 7. Magnetization of valley K as a function of twist angle θ and filling factor n/n_s . (a) Without gate field. (b) With gate field such that the interlayer on-site energy difference is $\Delta V = 100$ meV. Note that gate fields end to suppress the difference $|M_{c,t}^K - M_{c,b}^K|$, especially for small twist angles.

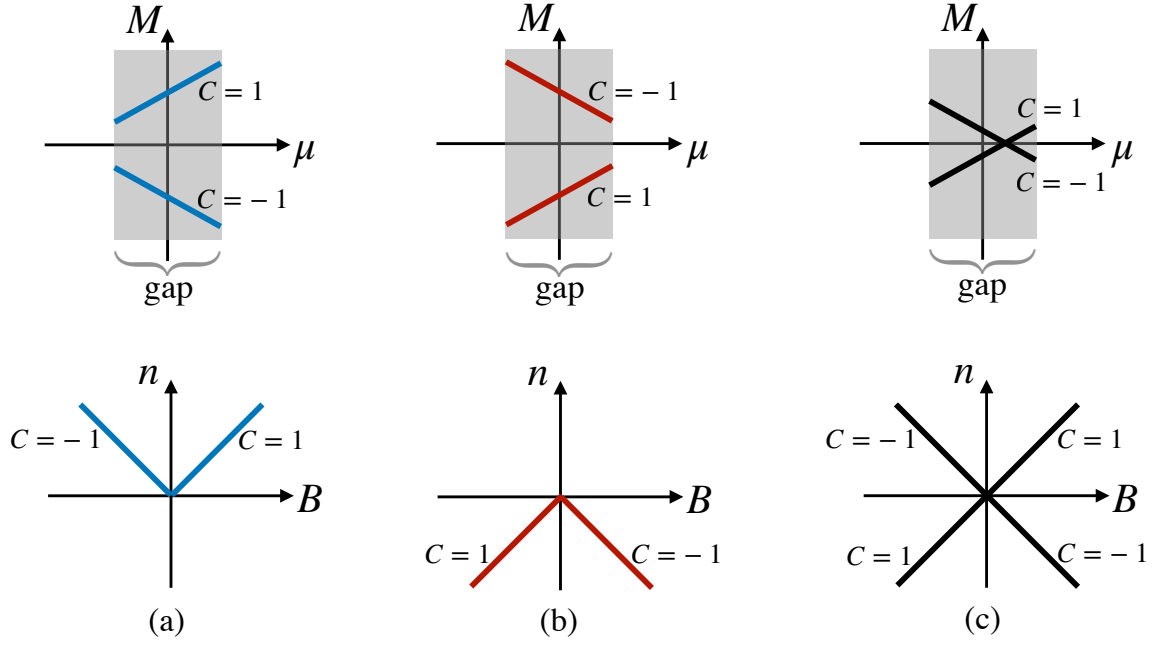


FIG. 8. Indication of the sign switch of magnetization M in Landau fans. (a) The sign of M does not change across the band gap and is the same as the sign of Hall conductivity. The anomalous quantum Hall state is more robust for n -doping. (b) The sign of M does not change across the band gap and is opposite to the sign of Hall conductivity. The anomalous quantum Hall state is more robust for p -doping. (c) The sign of M switches across the band gap. The anomalous quantum Hall state is equally robust for n - and p -doping.